A VLT/FORS2 NARROWBAND IMAGING SEARCH FOR MGII EMISSION AROUND Z∼0.7 GALAXIES

Ryan Rickards Vaught [1], Kate Rubin [1], Fabrizio Arrigoni Battaia [2], Xavier Prochaska, Joseph Hennawi

[1]San Diego State University 5500 Campanile Dr, San Diego, CA 92182

[2]Max-Planck-Institut fur Astronomie, Konigstuhl 17, D- 69117 Heidelberg, Germany

ABSTRACT

Galactic-scale outflows are thought to be the primary mechanism in the removal of cool gas in star-forming galaxies. Presently, the mass and energy of these flows remain poorly constrained. One way to better constrain these parameters is to measure the spatial extent of the outflow; however, measuring the spatial extent of such outflows via spectral methods has been traditionally very difficult due to the faintness of emission lines tracing outflowing material. We present VLT/FORS2 narrowband imaging of 5 star forming galaxies at redshift z=0.67-0.69 in the GOODS-S field as part of an effort to spatially resolve large-scale outflows traced by MgII emission. Previous spectra of this sample have already revealed winds traced by MgII absorption. At our sample redshift, the MgII emission lines fall exactly within the FORS2 HeII+47 and HeII/3000+48 interference filters. The total integration time of 10 hrs obtained in each filter permits the analysis of the flow surface brightness and extent on scales over which MgII is typically detected in absorption (i.e, projected distances ¿ 100 kpc). Such measurements can provide stronger constraints on the mass and energy of feedback, helping to advance our understanding of the processes regulating galaxy evolution up to z=1.

1. INTRODUCTION

Galactic scale outflows are considered to be the main driver of galaxy evolution, as they provide a means to transport cool gas away from star forming regions out to the intergalactic medium. In other words, this removal of cool gas carries away the necessary fuel that is required for stellar formation. Even though outflows play a critical role in the star formation rates and mass of a the host galaxy(Werk et al. 2014), the physical production mechanism that powers these outflows remains uncertain. Despite the uncertainty, some possible mechanics have been proposed by theoretical studies that include thermal pressure from core collapse supernova, radiation pressure from starbursts and finally cosmic ray pressure(Sugahara et al. 2017; Larson 1974; Chevalier & Clegg 1985; Springel & Hernquist 2003). An accurate picture of what types of galaxies host outflows comes from numerous spectroscopic studies(authors), as outflows are detected by measuring the blueshift of absorption transitions with respect to the host galaxy systematic velocities. Spectroscopy of galaxies from small to large redshifts and over a wide range of star formation sequence have revealed outflows in galaxies which host a large concentrations of massive stars (e.g., Rubin et al. (2014) Martin 2012).

One common practice in detecting the presence of gas in distant galaxies has been to spectroscopically probe galactic halos along background quasar sight lines and down-the-barrel observations. With temperatures of the cool halo gas component on the order of 10^4 K, the gas can be traced by the absorption of metals such Mg II, Fe and others (Bordoloi et al. 2011; Bergeron 1986). Nonetheless, this method is weak in constraining the overall radial profile, extent and morphology of the outflow. It follows from these weak constraints that estimates of mass and energy loss are left uncertain by at least two order of magnitude (Rubin et al. 2011).

In a study by Rubin et al. (2010) strong Mg II emission with a P-Cygni line profile was observed in the GOODS-N galaxy TKRS 4389. A proposed production mechanism for the observed Mg II emission is photon scattering.

2. OBSERVATIONS AND DATA REDUCTION

Our sample consists of 5 GOODS-S galaxies. These galaxies were selected from a Keck/LRIS survey of UV absorption lines in 100 objects having redshifts $0.3 < z, 1.4$ and $B_{AB} < 23$ in fields with deep HST/ACS imaging Rubin et al. (2014). The full sample is fortuitously distributed on the sky such that it can be imaged in a single FORS2 pointing.

The data were taken in service-mode using the FORS2 instrument on the VLT 8.2m telescope Antu between October 2012 and February 2013. We used two narrowband filters, HeII+47 and HeII/3000+48, that have peak transmission at wavelengths that correspond to the MgII doublet lines at our sample redshift of $z \approx 0.7$, (see Table 1). The FORS2 has a pixel scale of $0.25''$ pixel^{-1}

and a field of view of $7' \times 7'$. Summing the individual exposure times for each image results in a combined exposure time of 10.0 hours each for the HeII+47 and HeII/3000+48 filters. We carried out our observations under photometric and thin cloud conditions (program ID: 090.A-0427A).

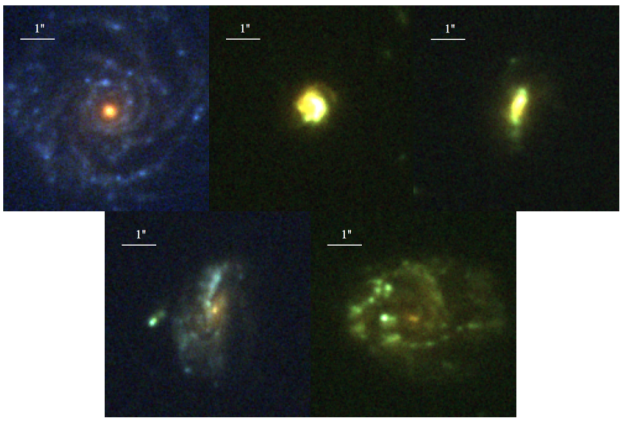

Figure 1. HST/ACS imaging of the each galaxy in our sample. From Top Left to Right Bottom: J033230.03, J033230.64, J033225.26, J033231.36, J033230.57.

The data were reduced using custom routines written in **Python**. The images were first corrected by subtracting and removing the overscan region of the CCD. Then the images were bias-subtracted and flat-fielded using twilight flats. Each individual image was cleaned of cosmic rays and bad pixels by utilizing the L.A Cosmic algorithm. The astrometry solutions were calculated via Astrometry.net (Lang et al. 2010) with a standard deviation in the galaxy coordinates of $\sigma \approx 0.10''$.

Before image stacking, we ran each frame through **SExtractor** (Bertin et al. 2002) in order to create a Root-Mean-Square map of each science image. These frames, in addition to the science images, are stacked to create a co-added RMS image.

The final stacked images for each filter is obtained using **SWarp** (Bertin et al. 2002). Each individual frame is first sky-subtracted using a background mesh size of 256 pixels which is approximately $64''$. We chose the mesh size to be large enough such that the extended emission is not mistakenly subtracted (Arrigoni Battaia et al. 2015). The frame, after background-subtraction, is resampled onto a common astrometric solution using a *Lancosz3* interpolation kernel. The images are median-combined in order to increase the signal to noise of any MgII emission. **SWarp** is also configured to produce RMS weight map from our **SExtractor** weighted images.

Once image stacking was done, we were left with two images to perform photometry on. One image contains only continuum photons, while the other one contains

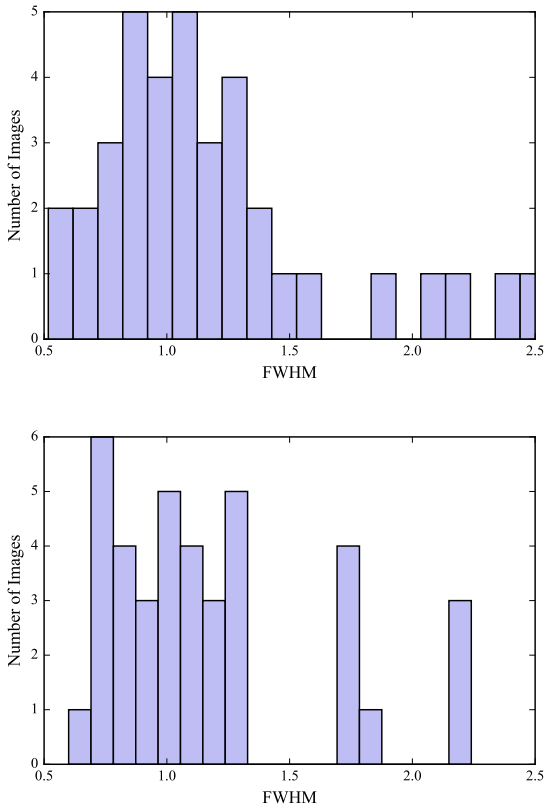

Figure 2. The seeing conditions were calculated by ESO and were provided in the header of each science image. **(Top)** Distribution of seeing for the HeII+47 images. The median seeing is $1.03''$ **(Bottom)** : Same for the HEII/3000+48 images. The median seeing is $1.08''$

continuum + MgII photons. (see Figure 3). One side effect from stacking is that the east and west borders of each image contain greater noise compared to the center of the image. This is due to the imperfect overlap of the 3 pointings used. However, the sample galaxies are sufficiently distant from these low S/N regions that their photometry is not affected. As a final step, both images are aligned in physical coordinates via the IRAF **Imalign** command (Tody 1986).

Table 1. VLT/FORS2 Observations: Filter and exposure properties of the VLT observations. The width of the transmission curves are calculated by convolving the transmission curve with the total wavelength range of the filter. These values differ slightly from those reported by the European Space Observatory.

Filter	λ_{eff}(Å)[a]	λ_{width}(Å)	N_{images}	$t_{tot}(s)$	S[b] $\times 10^{-17}$
HeII	4675.21	50.11	38	35,959	2.45
HeII/3000	4722.46	44.82	38	36,937	2.40

[a] λ_{eff} is the effective wavelength of the filter transmission curve.

[b] S is in units of ergs counts^{-1} cm^{-2}

2.1. *Supplemental Keck/LRIS spectra*

In addition to VLT imaging, we utilize galaxy spectra taken from the Rubin et al. (2014) Keck I Low Resolution Imaging Spectrometer (LRIS) program. A 0.9″ slit width was used for all slitmasks and the median FWHM resolution for the spectra is 274 km s^{-1} at λ rest $\approx$ 2800 Åand 286 km s^{-1} at λ rest $\approx$ 2600 Å, see Figure (6).

2.2. *Absolute Flux Calibration*

We acquired observations of the standard star GD50 from archival ESO calibration imaging. From this standard we calculated the atmospheric extinction coefficients to be 0.181 magnitudes for the HeII/3000+48 filter and 0.190 magnitudes for the HeII+47 filter. Since we have imaging of the standard star GD50 in our two filters, and access to GD50's spectral energy distribution and each filters transmission curve through the ESO website, we are able to perform absolute flux calibration using the methods of Jacoby et al. (1990). We first convolve the spectral energy distribution of the standard star, $F(\lambda)$ in ergs sec^{-1} Å^{-1} cm^{-2}, with that of the known transmission curve of the filter, $T_i(\lambda)$. This yeilds, F_i, the total observable flux in each bandpass filter i with units of ergs sec^{-1} cm^{-2}.

$$F_i = \int F(\lambda) T_i(\lambda) d\lambda$$

It is not uncommon to assume that $F(\lambda)$ is constant over the small width of the filter. However, our filter transmission curves are sampled at 5 Å intervals which is the same sampling as the spectral energy distribution of the standard star obtained from the ESO archives. Therefore we calculate the integral numerically. The system sensitivity, including the defects of the telescope optics and detector response is then given by

$$S_i = \frac{F_i}{C 10^{k_i A}},$$

where k_i is the extinction in magnitudes per airmass, A is the airmass for each individual exposure, C is the measured count rate of the standard star and S is in units of ergs counts^{-1} cm^{-2}. Before image co-addition, each science image is corrected for atmospheric extinction by multiplying each frame by $10^{k_i A}$. Next, the image is divided by the exposure time, effectively putting the image in units of counts per sec. After co-addition, the images are then multiplied by the appropriate sensitivity factor S_i. This puts the final images in the appropriate flux units ergs sec $^{-1}$ cm^{-2}.

3. ANALYSIS

3.1. *Spectral Correction*

With the supplementary spectra from Rubin et al. (2014), we can fit the continuum and determine the slope of each galaxy spectrum in order to determine if the spectral slope gives rise to differences in continuum flux between the two filters. We use the interactive fitting routine **lt_continuumfit** from the linetools package (Prochaska et al. 2016)[1] to fit the continuum. By fitting the continuum we are masking the absorption features and making an effectively flat spectrum, which we use as a model. We find the total flux in each filter by convolving the fitted continuum with each filter's transmission curve. Next, we take the ratio of both integrated totals, as the ratio will indicate the scaling factor needed to correct either of the filters. Comparing these ratios between each galaxy, we find that each ratio is effectively the same, within 1/1000 percent, with a value of 1.118. This value is equal to the ratio between the FWHM of the transmission curves, allowing us to conclude that the slope of the spectrum of each galaxy does not affect the continuum values collected in either filter.

3.2. *Continuum Subtraction*

To properly continuum-subtract the image taken with the emission filter in excess of the continuum, we follow a prescription given by Arrigoni Battaia et al. (2015). We first determine the continuum flux density from the off-Mg II filter,

$$f_{cont} = \frac{F_{cont}}{\Delta\lambda_{cont}}, \quad (1)$$

where F_{cont} and $\Delta\lambda_{cont}$ are the observed flux per pixel of the continuum image per pixel and the transmission FWHM of the continuum filter, respectively. With f_{cont} it is then possible to calculate the flux of any excess emission, F_{line}:

$$F_{line} = F_{MgII} - f_{cont}\Delta\lambda_{MgII} \quad (2)$$

where F_{MgII} and $\Delta\lambda_{MgII}$ are the observed flux per pixel in the Mg II filter and the transmission FWHM of the Mg II filter. The continuum subtracted images of each galaxy are shown in Fig. 5.

3.3. *Surface Brightness Profiles and Limits*

In order to test for the presence of Mg II emission, we perform aperture photometry on the continuum subtracted images using the python library Photutils. We choose apertures with thickness of 2 pixels or 0.50″, such that, $r_{inner} = r_{outer} - 2$ (in pixels). Each aperture is centered on the flux-weighted centroid of the galaxy. We also consider an aperture with an inner radius of 24 pixels (6″) and outer radius of 30 pixels (7.5″) in order to increase our sensitivity to extended emission. Dividing

[1] https://github.com/linetools/linetools

Table 2. Properties of 5 galaxies in our sample : These properties were taken from Rubin et al. (2014). All galaxies are at roughly the same redshift. The star formation rates for the sample range from 3.8 to 40.5 solar mass per year. The EW are for the blended components of the MgII doublet and were calculated with Eq. 3 and the supplemental Keck/LRIS spectra

Object	R.A.	Dec	z	SFR($M_\odot yr^{-1}$)	$\log M_*/M_\odot$	EW(Å)
J033225.26-274524.0	03:32:25.26	-27:45:23.9	0.6660	$9.1^{+1.3}_{-3.7}$	$9.86^{+0.05}_{-0.04}$	7.00 ± 0.51
J033231.36-274725.0	03:32:31.35	-27:47:24.9	0.6669	$10.5^{+1.7}_{-1.6}$	$10.02^{+0.03}_{-0.03}$	6.50 ± 0.51
J033230.03-274347.3	03:32:30.03	-27:43:47.2	0.6679	3.8^{+0}_{-0}	$10.98^{+0.01}_{-0.0}$	6.44 ± 0.51
J033229.64-274242.6	03:32:29.64	-27:42:42.5	0.6671	$40.5^{+8.2}_{-12.1}$	$10.30^{+0.07}_{-0.03}$	6.70 ± 0.51
J033230.57-274518.2	03:32:30.56	-27:45:18.2	0.6807	$12.6^{+1.7}_{-2.1}$	$10.48^{+0.03}_{-0.07}$	5.60 ± 0.52

the summed flux in each aperture by the area in arcsecs we produced surface brightness (SB) profiles for each galaxy.

The error bars are determined from a weight image produced by **SWarp**. The weight image is converted to an RMS image by taking the square root of the inverse weight. We then place apertures that are identical to the apertures used to find the SB profiles for each galaxy. To calculate the variance inside each aperture, we sum the RMS pixel values in quadrature, then divide by the area of each aperture.

To calculate the 3σ SB detection limit in each filter, we first masked out all the sources, their associated extended halos, and edge noise in both the HE+47 and HE/3000+48 images. We then calculated the root-mean-square of the background in randomly placed apertures with radii that matched the aperture radii used to measure the SB of the galaxies. The RMS values were then converted into SB in 1 square arcsec apertures. These values are calculated to be 5.120×10^{-18} ergs sec $^{-1}$ cm^{-2} arcsec^2 and 4.154×10^{-18} ergs sec $^{-1}$ cm^{-2} arcsec^2 in the HeII/3000 and HeII filters, respectively. We repeated the above procedure to obtain SB limits for the set of continuum-subtracted images: we calculated the root-mean-square of the flux inside the largest aperture. We determined the 3σ SB limits to be 2.09×10^{-18}ergs sec $^{-1}$ cm^{-2} arcsec^2 and 1.87×10^{-18} ergs sec $^{-1}$ cm^{-2} arcsec^2 for the HeII - HeII/3000 combination and the HeII/3000 - HeII combination.

3.4. *Equivalent Widths*

Here we derive an expression to calculate the equivalent width (EW) of any absorption or emission features observed in our narrow-band imaging. Start from the expression for EW used in the context of spectroscopy,

$$EW = \int (1 - \frac{f_{line}}{f_{cont}}) d\lambda \tag{3}$$

We begin by dividing Eq 2 by the flux density of the continuum and the FWHM of the on-line filter,

$$\frac{F_{line}}{f_{cont}\Delta\lambda_{MgII}} = \frac{F_{MgII}}{f_{cont}\Delta\lambda_{MgII}} - 1 \tag{4}$$

Next, we rearrange the above expression such that we produce the argument of the integrand in Eq. 3 on the RHS,

$$-\frac{F_{line}}{f_{cont}\Delta\lambda_{MgII}} = 1 - \frac{f_{MgII}}{f_{cont}}. \tag{5}$$

We then approximate the integration in Eq. 3 by multiplying the integrand above by the FWHM of the on-line filter $d\lambda = \Delta\lambda_{MgII}$,

$$-\frac{F_{line}}{f_{cont}} = (1 - \frac{f_{MgII}}{f_{cont}})\Delta\lambda_{MgII}; \tag{6}$$

such that

$$EW = -\frac{F_{line}}{f_{cont}}. \tag{7}$$

Using the above equation along with the continuum and continuum subtracted images, we produce images of the of equivalent widths. The EW are displayed inside a 1σ SB contour of Continuum flux. Outside this contour, the EW become large due to the lack of S/N on the continuum, see Figure 7.

4. RESULTS

In this section we present the results from the continuum-subtraction of the off-line continuum filter to that of the on-line emission filter.

4.1. *Limits on the MgII emission*

The surface brightness profiles presented in Fig. 4 do not exhibit any signs of extended MgII emission. Previous constraints on the brightness of any possible emission are given by (Rubin et al. 2011). In this work the authors studied emission in a starburst galaxy at

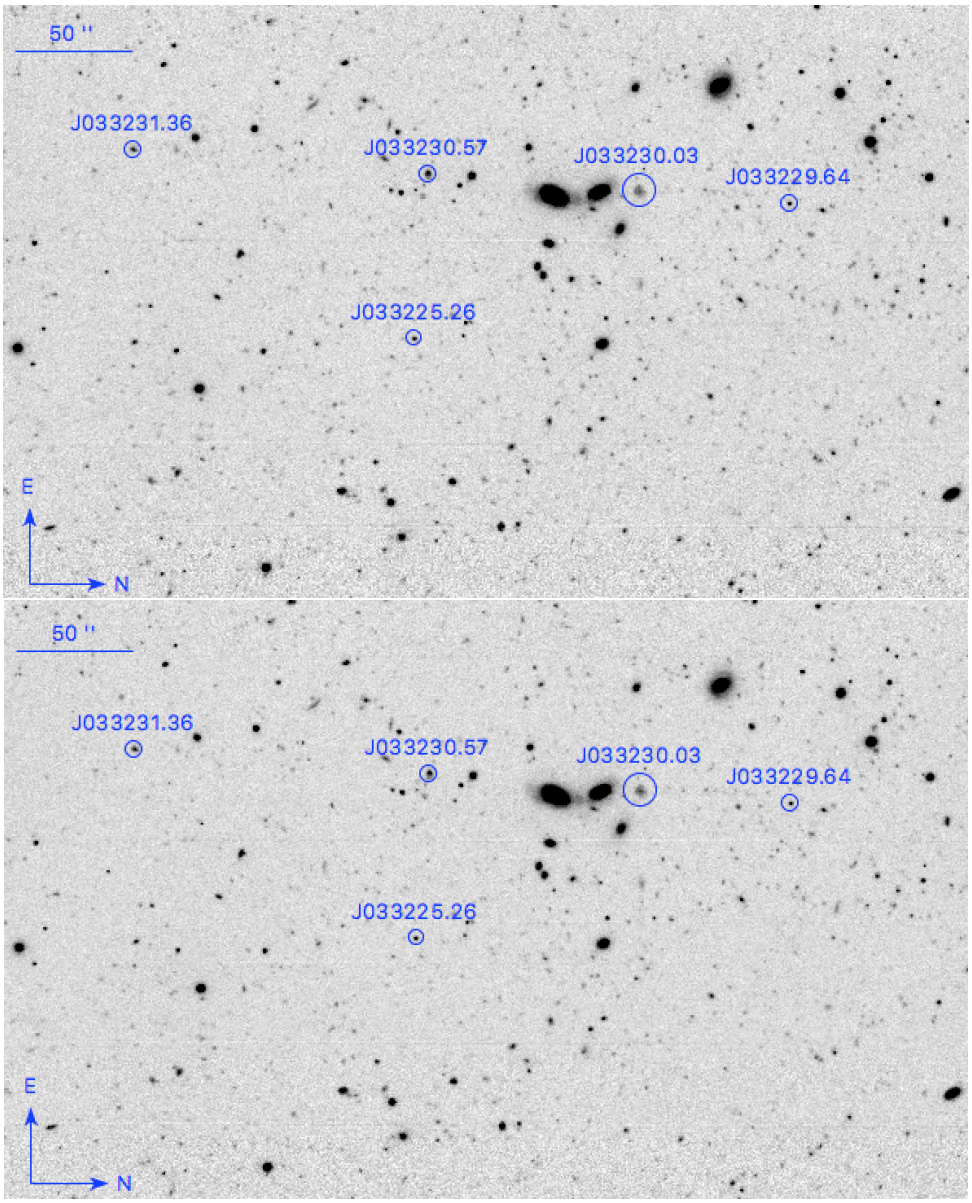

Figure 3. Top: HeII+47 image after stacking. Bottom: HeII3000+48 image after stacking.

$z = 0.69$ with a star formation rate of 80 $M_{\odot} yr^{-1}$. In a two-dimensional Keck/LRIS spectrum of this galaxy, they measured fluxes of 4.04 ± 0.4 to 8.0 ± 0.4 10^{-18}ergs sec $^{-1}$ cm^{-2} above and below the continuum region of the 2D spectra at λ2796. Converting the 3σ detection limit of our continuum-subtracted MgII image into flux units, we report the MgII emission 3σ limits as 5.37 10^{-18}ergs sec $^{-1}$ cm^{-2}. Comparing our SB limit to previously reported values, it should be possible to detect the emission of this galaxy.

4.2. *MgII absorption in the line-profile*

Although we do not measure any extended MgII emission, we do observe a decrement of flux in the galaxy continua measured in the MgII filter in 3 galaxies out of the 5 galaxy sample. In the following section we discuss the absorption in each of these three galaxies, as well as our null detections.

We first discuss the case of a null detection of MgII absorption. The galaxy J033230.57 at a redshift of $z = 0.6807$ is the most redshifted galaxy of the sample. This galaxy shows no significant flux decrement in the MgII filter. Examining Figure **??**, we can see that there should not be any absorption measured in J033230.57, as the absorption profile in the spectrum appears both in the HeII and HeII/3000 filter. This is a good test of our flux calibration, as it appears that there are no hints of systematic false absorption signatures.

We have a second case in which we detect quite strong absorption. The galaxy J033230.64 exhibits a maximum

flux decrement of roughly 4×10^{-18} ergs sec $^{-1}$ cm^{-2} arcsec^{-1} due to Mg II absorption. The absorption is exhibited predominantly within the 1σ SB outline of the continuum. The mean value of the EW in all the pixels within the 1σ SB outline of this galaxy is 7.88 ± 0.403 Å, which is relatively close to the EW calculated from the spectra, 6.70 ± 0.51 Å. We expect that the small difference is due to the collecting area of the different methods. We calculate the EW inside a 1σ region around the core of the galaxy, whereas the spectrim is obtained in a $0.9''$ slit width. In addition, further inspecting of the distribution of the EW over the pixels, there appear to be two outlier values of $EW \approx 20$ Åthat are influencing the mean value.

The next galaxy that shows an decrement of flux from MgII absorption is J033231.36. The MgII absorption spills outside the 1σ continuum flux contour, however a significant amount lies within our 1σ significant detection. The mean value of the EW of this galaxy is 6.91 ± 0.560 Å, and is in good agreement with the EW calculated from the Keck/LRIS spectra, 6.50 ± 0.51 Å. Again, inspection of the distribution of the EW over the pixels, reveal a possible outlier of an $EW \approx 20$ Å.

5. ANALYSIS

6. CONCLUSION

We presented the results of a narrowband imaging search for MgII emission in a sample of GOODS-S galaxies at a redshift of $z \approx 0.70$. Although we were unable to detect any measurable amount of MgII emission, We were able to detect a non-trivial amount of MgII absorption in 3 of our 5 galaxy sample. Our images, which are effective in creating absorption maps, were used to calculate the EW of absorption inside a 1σ continuum contour.

REFERENCES

Arrigoni Battaia, F., Yang, Y., Hennawi, J. F., et al. 2015, ApJ, 804, 26

Bergeron, J. 1986, A&A, 155, L8

Bertin, E., Mellier, Y., Radovich, M., et al. 2002, in Astronomical Society of the Pacific Conference Series, Vol. 281, Astronomical Data Analysis Software and Systems XI, ed. D. A. Bohlender, D. Durand, & T. H. Handley, 228

Bordoloi, R., Lilly, S. J., Knobel, C., et al. 2011, ApJ, 743, 10

Chevalier, R. A., & Clegg, A. W. 1985, Nature, 317, 44

Lang, D., Hogg, D. W., Mierle, K., Blanton, M., & Roweis, S. 2010, AJ, 139, 1782

Larson, R. B. 1974, Monthly Notices of the Royal Astronomical Society, 169, 229

Rubin, K. H. R., Prochaska, J. X., Koo, D. C., et al. 2014, ApJ, 794, 156

Rubin, K. H. R., Prochaska, J. X., Koo, D. C., Phillips, A. C., & Weiner, B. J. 2010, The Astrophysical Journal, 712, 574

Rubin, K. H. R., Prochaska, J. X., Ménard, B., et al. 2011, ApJ, 728, 55

Springel, V., & Hernquist, L. 2003, Monthly Notices of the Royal Astronomical Society, 339, 289

Sugahara, Y., Ouchi, M., Lin, L., et al. 2017, ApJ, 850, 51

Tody, D. 1986, in Proc. SPIE, Vol. 627, Instrumentation in astronomy VI, ed. D. L. Crawford, 733

Werk, J. K., Prochaska, J. X., Tumlinson, J., et al. 2014, ApJ, 792, 8

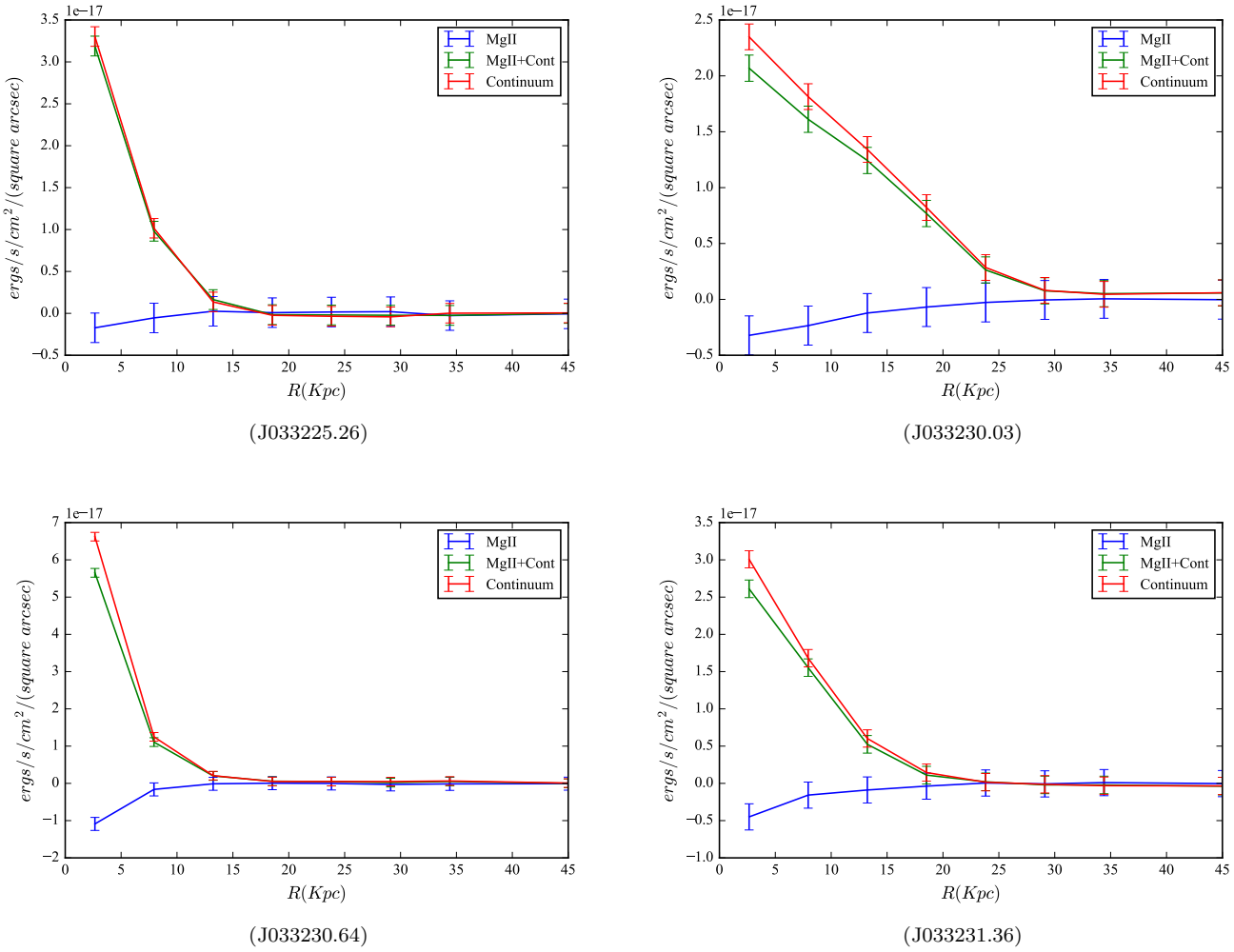

Figure 4. Surface brightness profiles for galaxies that exhibit flux decrements from MgII absorption. Photometry was performed with circular apertures with increasing inner and outer radii. The error bars are determined from a SWarp RMS map .

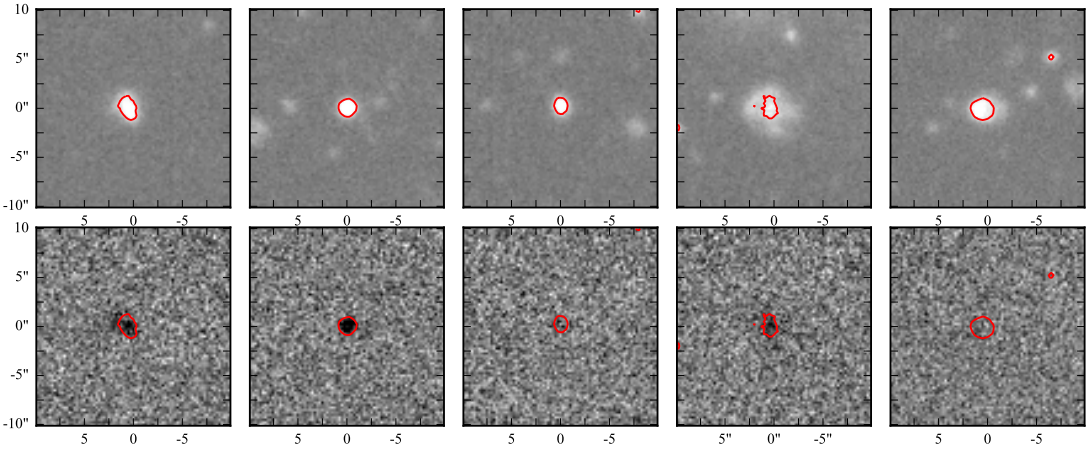

Figure 5. $10'' \times 10''$ images stamps. Bottom: Continuum flux in ergs/s/cm^2/arcsec. Top: Continuum subtracted MgII flux, absorption can be seen in 3 of 5 galaxies. Each stamp is scaled with symmetric limits around 0.

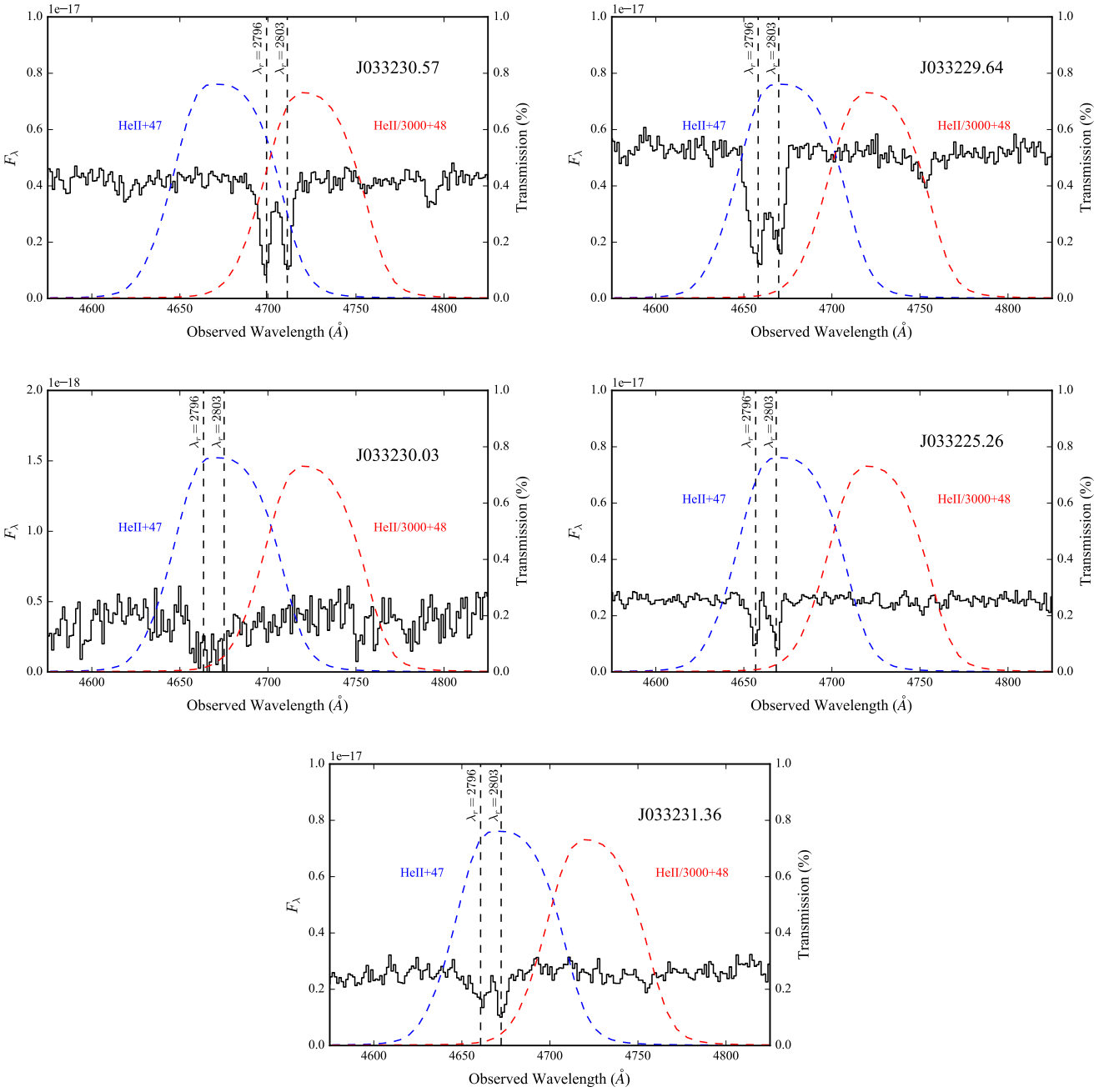

Figure 6. KECK/LRIS spectra plotted with the transmission curves of the filters HeII+47 and HeII/3000+48. The MgII doublet falls fortuitously the central wavelength of the HEII+47 filter.

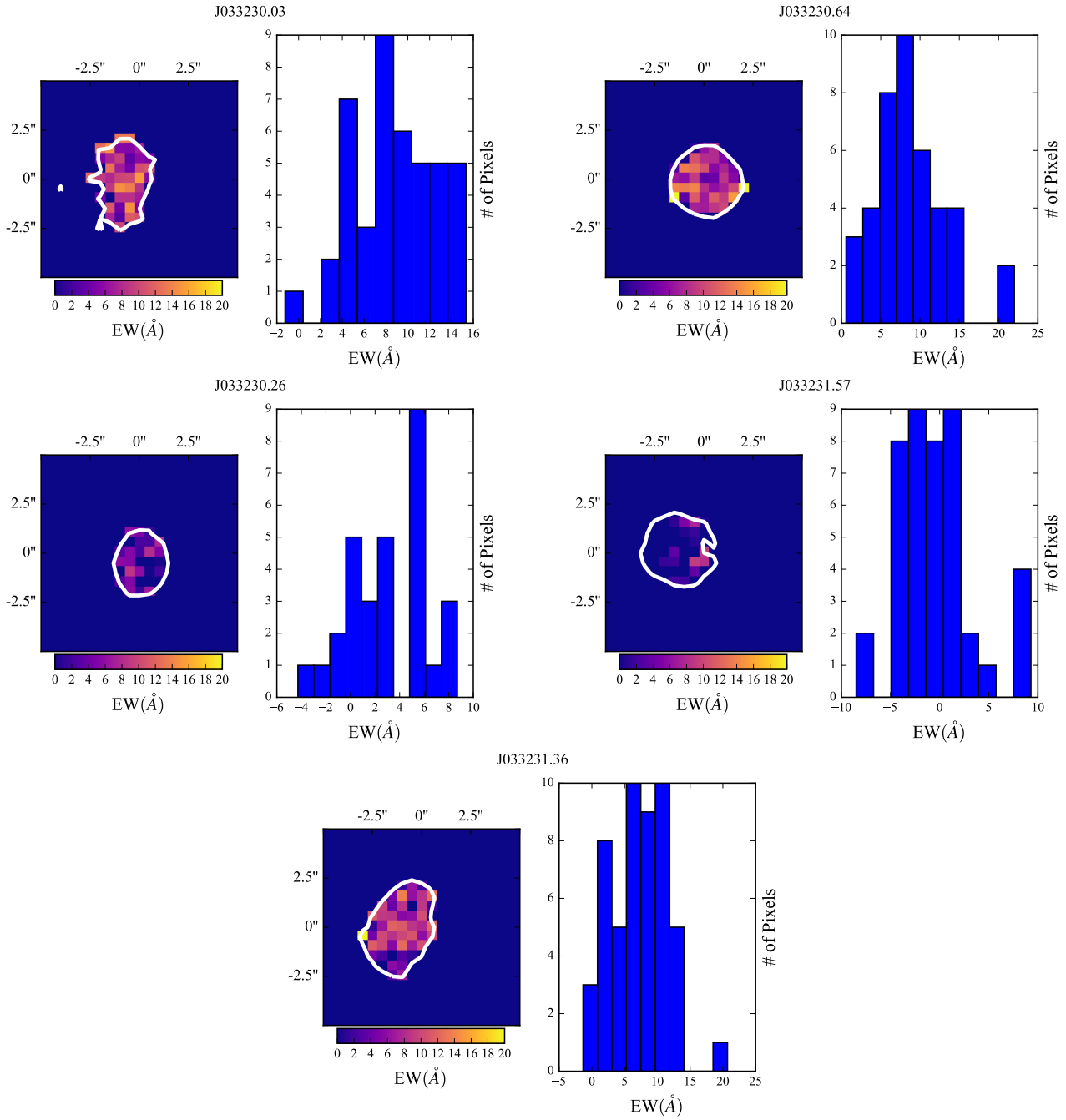

Figure 7. Plots of the distribution of equivalent widths inside a 1σ continuum flux outline.